The depolarization–attenuated backscatter relationship for dust plumes

Tian Zhou, Jianping Huang,* Zhongwei Huang, Jingjing Liu, Wencai Wang, and Lei Lin

Key Laboratory for Semi-Arid Climate Change of the Ministry of Education, College of Atmospheric Sciences, Lanzhou University, Lanzhou, 730000, China

**hjp@lzu.edu.cn*

Abstract: This study identified the relationship between the layer-integrated attenuated backscatter coefficient and layer-integrated depolarization ratio of dust plumes and compared it with that of cloud, using CALIPSO LIDAR measurements. The histogram distribution of the integrated color ratio for dust and cloud was also examined. On the basis of the layer-integrated attenuated backscatter coefficient and layer-integrated depolarization ratio relation, a simple method of detecting dust plumes was developed. A case study of dust identification over the Taklimakan Desert was conducted and compared with the current CALIPSO products. The result shows that the proposed method can significantly improve the classification of cloud and dust plumes and can supplement the current space-borne LIDAR discrimination approach, especially over dust source regions. In addition, The zonal and meridional mean occurrence derived by the proposed method and the CALIPSO's method were compared for Asian dust over East Asia region (30°N −45°N, 80°E −180°E) using the night measurements of CALIPSO from March to May, 2007. The comparison showed that the dust occurrence obtained from the proposed method is larger than that of CALIPSO's method. The dust could be found up to around 6-8 km (Above Sea Level, ASL) near the Taklimakan desert region, and maximum occurrence is over 80%. The transport altitude remained at 3km-7km (ASL) as the dust was transported across the Pacific Ocean.

OCIS codes: (010.0280) Remote sensing and sensors; (010.1100) Aerosol detection; (010.1350) Backscattering; (010.3640) Lidar.

References and links

1. S. Twomey, M. Piepgrass, and T. L. Wolfe, "An assessment of the impact of pollution on global cloud albedo," Tellus **36B**(5), 356–366 (1984).
2. A. Slingo, T. P. Ackerman, R. P. Allan, E. I. Kassianov, S. A. McFarlane, G. J. Robinson, J. C. Barnard, M. A. Miller, J. E. Harries, J. E. Russell, and S. Dewitte, "Observations of the impact of a major Saharan dust storm on the atmospheric radiation balance," Geophys. Res. Lett. **33**(24), L24817 (2006), doi:10.1029/2006GL027869.
3. J. Huang, B. Lin, P. Minnis, T. Wang, X. Wang, Y. Hu, Y. Yi, and K. Ayers, "Satellite-based assessment of possible dust aerosols semi-direct effect on cloud water path over east Asia," Geophys. Res. Lett. **33**(19), L19802 (2006a), doi:10.1029/2006GL026561.
4. J. Huang, Q. Fu, J. Su, Q. Tang, P. Minnis, Y. Hu, Y. Yi, and Q. Zhao, "Taklimakan dust aerosol radiative heating derived from CALIPSO observations using the Fu-Liou radiation model with CERES constraints," Atmos. Chem. Phys. **9**(12), 4011–4021 (2009).
5. Z. Huang, J. Huang, J. Bi, G. Wang, W. Wang, Q. Fu, Z. Li, S.-C. Tsay, and J. Shi, "Dust aerosol vertical structure measurements using three MPL lidar during 2008 China-U.S. joint dust field experiment," J. Geophys. Res. **115**, D00K 15, doi:10.1029/2009JD013273 (2010).
6. Z. Liu, A. Omar, M. Vaughan, J. Hair, C. Kittaka, Y. Hu, K. Powcell, C. Trepte, D. Winker, C. Hostetler, R. Ferrare, and R. Pierce, "CALIPSO lidar observations of the optical properties of Saharan dust: a case study of long-range transport," J. Geophys. Res. **113**(D7), D07207 (2008), doi:10.1029/2007JD008878.
7. J. M. Haywood, V. Ramaswamy, and B. J. Soden, "Tropospheric aerosol climate forcing in clear-sky satellite observations over the oceans," Science **283**(5406), 1299–1303 (1999).

8. A. Higurashi and T. Nakajima, “Detection of aerosol types over the east China sea near Japan from four-channel satellite data,” Geophys. Res. Lett. **29**(17), 1836 (2002), doi:10.1029/2002GL015357.
9. T. Takemura, I. Uno, T. Nakajima, A. Higurashi, and I. Sano, “Modeling study of long-range transport of Asian dust and anthropogenic aerosol from east Asia,” Geophys. Res. Lett. **29**(24), 2158 (2002), doi:10.1029/2002GL016251.
10. J. Huang, P. Minnis, B. Chen, Z. Huang, Z. Liu, Q. Zhao, Y. Yi, and J. K. Ayers, “Long-range transport and vertical structure of Asian dust from CALIPSO and surface measurements during PACDEX,” J. Geophys. Res. **113**(D23), D23212 (2008).
11. I. Uno, K. Eguchi, K. Yumimoto, T. Takemura, A. Shimizu, M. Uematsu, Z. Liu, Z. Wang, Y. Hara, and N. Sugimoto, “Asian dust transported one full circuit around the globe,” Nature, doi:10.1038/NGEO583(2009).
12. J. Huang, P. Minnis, Y. Yi, Q. Tang, X. Wang, Y. Hu, Z. Liu, K. Ayers, C. Trepte, and D. Winker, “Summer dust aerosols detected from CALIPSO over the Tibetan Plateau,” Geophys. Res. Lett. **34**(18), L18805 (2007), doi:10.1029/2007GL029938.
13. Z. Liu, D. Liu, J. Huang, M. Vaughan, I. Uno, N. Sugimoto, C. Kittaka, C. Trepte, Z. Wang, C. Hostetler, and D. Winker, “Airborne dust distribution over the Tibetan Plateau and surrounding areas derived from the first year of CALIPSO lidar observations,” Atmos. Chem. Phys. **8**(16), 5045–5060 (2008).
14. K. Wang, Y. Zhang, A. Nenes, and C. Fountoukis, “Implementation of dust emission and chemistry into the Community Multiscale Air Quality modeling system and initial application to an Asian dust storm episode,” Atmos. Chem. Phys. **12**(21), 10209–10237 (2012).
15. N. Sugimoto, I. Uno, M. Nishikawa, A. Shimizu, I. Matsui, X. Dong, Y. Chen, and H. Quan, “Record heavy Asian dust in Beijing in 2002: observations and model analysis of recent events,” Geophys. Res. Lett. **30**(12), 1640 (2003), doi:10.1029/2002GL016349.
16. N. Sugimoto, Z. Huang, T. Nishizawa, I. Matsui, and B. Tatarov, “Fluorescence from atmospheric aerosols observed with a multi-channel lidar spectrometer,” Opt. Express **20**(19), 20800–20807 (2012).
17. N. Sugimoto, Y. Hara, A. Shimizu, T. Nishizawa, I. Matsui, and M. Nishikawa, “Analysis of dust events in 2008 and 2009 using the lidar network, surface observations and the GFORS model,” Asia-Pacific J. Atmos. Sci. **49**(1), 27–39 (2013).
18. K. Sassen, P. J. DeMott, J. M. Prospero, and M. R. Poellot, “Saharan dust storms and indirect aerosol effects on clouds: CRYSTAL-FACE results,” Geophys. Res. Lett. **30**(12), 1633 (2003), doi:10.1029/2003GL017371.
19. J. Huang, P. Minnis, B. Lin, T. Wang, Y. Yi, Y. Hu, S. Sun-Mack, and K. Ayers, “Possible influences of Asian dust aerosols on cloud properties and radiative forcing observed from MODIS and CERES,” Geophys. Res. Lett. **33**(6), L06824 (2006b), doi:10.1029/2005GL024724.
20. J. Su, J. Huang, Q. Fu, P. Minnis, J. Ge, and J. Bi, “Estimation of Asian dust aerosol effect on cloud radiation forcing using Fu-Liou radiative model and CERES measurements,” Atmos. Chem. Phys. **8**(10), 2763–2771 (2008).
21. W. Wang, J. Huang, P. Minnis, Y. Hu, J. Li, Z. Huang, J. K. Ayers, and T. Wang, “Dusty cloud properties and radiative forcing over dust source and downwind regions derived from A-Train data during the Pacific dust experiment,” J. Geophys. Res. **115**, D00H35 (2010), doi:10.1029/2010JD014109.
22. M. S. Jphnson, N. Meskhidz, V. P. Kiliyanpilakkil, and S. Gasso, “Understanding the transport of Patagonian dust and its influence on marine biological activity in the South Atlantic Ocean,” Atmos. Chem. Phys. **11**(6), 2487–2502 (2011).
23. M. Schulz, J. M. Prospero, A. R. Baker, F. Dentener, L. Ickes, P. S. Liss, N. M. Mahowald, S. Nickovic, C. P. García-Pando, S. Rodríguez, M. Sarin, I. Tegen, and R. A. Duce, “Atmospheric transport and deposition of mineral dust to the ocean: implications for research needs,” Environ. Sci. Technol. **46**(19), 10390–10404 (2012).
24. D. M. Winker, W. H. Hunt, and M. J. McGill, “Initial performance assessment of CALIOP,” Geophys. Res. Lett. **34**(19), L19803 (2007), doi:10.1029/2007GL030135.
25. D. Liu, Z. Wang, Z. Liu, D. Winker, and C. Trepte, “A height resolved global view of dust aerosols from the first year CALIPSO lidar measurements,” J. Geophys. Res. **113**(D16), D16214 (2008), doi:10.1029/2007JD009776.
26. A. Omar, Z. Liu, M. Vaughan, Y. Hu, S. Ismail, K. Powell, D. Winker, C. Trepte, and B. E. Anderson, “Extinction-to-backscatter ratios of Saharan dust layers derived from in situ measurements and CALIPSO overflights during NAMMA,” J. Geophys. Res. **115**(D24), D24217 (2010).
27. Z. Liu, D. Winker, A. Omar, M. Vaughan, C. Trepte, Y. Hu, K. Powell, W. Sun, and B. Lin, “Effective lidar ratios of dense dust layers over North Africa derived from the CALIOP measurements,” J. Quant. Spectrosc. Radiat. Transf. **112**(2), 204–213 (2011).
28. Y. Hu, Z. Liu, D. Winker, M. Vaughan, V. Noel, L. Bissonnette, G. Roy, and M. McGill, “Simple relation between lidar multiple scattering and depolarization for water clouds,” Opt. Lett. **31**(12), 1809–1811 (2006a).
29. Y. Hu, M. A. Vaughan, D. M. Winker, Z. Liu, and V. Noel, “A simple multiple scattering-depolarization relation of water clouds and its potential applications,” *Proceedings of 23nd International Laser Radar Conference*, Nara Japan, 19–22 (2006b).
30. Y. Hu, M. Vaughan, Z. Liu, B. Lin, P. Yang, D. Flittner, B. Hunt, R. Kuehn, J. Huang, D. Wu, S. Rodier, K. Powell, C. Trepte, and D. Winker, “The depolarization - attenuated backscatter relation: CALIPSO lidar measurements vs. theory,” Opt. Express **15**(9), 5327–5332 (2007).
31. H. M. Cho, P. Yang, G. W. Kattawar, S. L. Nasiri, Y. Hu, P. Minnis, C. Trepte, and D. Winker, “Depolarization ratio and attenuated backscatter for nine cloud types: analyses based on collocated CALIPSO lidar and MODIS measurements,” Opt. Express **16**(6), 3931–3948 (2008).

#188543 - $15.00 USD Received 9 Apr 2013; revised 27 May 2013; accepted 5 Jun 2013; published 18 Jun 2013

32. D. M. Winker, J. Pelon, J. A. Coakiey, Jr., S. A. Ackerman, R. J. Charlson, P. R. Colarco, P. Flamant, Q. Fu, R. M. Hoff, C. Kittaka, T. L. Kubar, H. Le Treut, M. P. Mccormick, G. Megie, L. Poole, K. Powell, C. Trepte, M. A. Vaughan, and B. A. Wielicki, "The CALIPSO MISSION: a global 3D view of aerosols and clouds," Bull. Amer. Meteor. Soc. doi: 10.1175/2010BAMS3009 (2010).
33. D. M. Winker, M. A. Vaughan, A. Omar, Y. X. Hu, and K. A. Powell, "Overview of the CALIPSO mission and CALIOP data processing algorithms," J. Atmos. Ocean. Techn. **26**(11), 2310, doi:10.1175/2009JTECHA128.1 (2009).
34. L. Adhikari, Z. Wang, and M. Deng, "Seasonal variations of Antarctic clouds observed by CloudSat and CALIPSO satellite," J. Geophys. Res. **117**(D4), D04202 (2012), doi:10.1029/2011JD016719.
35. M. A. Vaughan, D. M. Winker, and K. A. Powell, *Part 2: Feature Detection and Layer Properties Algorithms* (CALIOP Algorithm Theoretical Basis Document, 2005).
36. U. Wandinger, M. Tesche, P. Seifert, A. Ansmann, D. Muller, and D. Althausen, "Size matters: influence of multiple scattering on CALIPSO light-extinction profiling in desert dust," Geophys. Res. Lett. **37**(10), L10801 (2010), doi:10.1029/2010GL042815.
37. W. Yang, A. Marshak, T. Varnai, O. V. Kalashnikova, and A. B. Kostinski, "CALIPSO observations of transatlantic dust: vertical stratification and effect of clouds," Atmos. Chem. Phys. **12**(23), 11339–11354 (2012).
38. M. Vaughan, S. Young, D. Winker, K. Powell, A. Omar, Z. Liu, Y. Hu, and C. Hostetler, "Fully automated analysis of space-based lidar data: an overview of the CALIPSO retrieval algorithms and data products," SPIE Int. Soc. Opt. Eng. **5575**, 16–30 (2004).
39. Z. Liu, M. Vaughan, D. Winker, C. Kittaka, B. Getzwich, R. Kuehn, A. Omar, K. Powell, C. Trepte, and C. Hostetler, "The CALIPSO lidar cloud and aerosol discrimination: vertion 2 algorithm and initial assessment of performance," J. Atmos. Ocean. Technol. **26**(7), 1198–1213 (2009).
40. G. Pappalardo, U. Wandinger, L. Mona, A. Hiebsch, I. Mattis, A. Amodeo, A. Ansmann, P. Seifert, H. Linne, A. Apituley, L. A. Arboledas, D. Balis, A. Chailovsky, G. D'Amico, F. D. Tomasi, V. Freudenthaler, E. Giannakaki, A. Giunta, I. Grigorov, M. Iarlori, F. Madonna, R. E. Mamouri, L. Nasti, A. Papayannis, A. Pietruczuk, M. Pujadas, V. Rizi, F. Rocadenbosch, F. Russo, F. Schnell, N. Spinelli, X. Wang, and M. Wiegner, "EARLINET correlative measurements for CALIPSO: First intercomparison results," J. Geophys. Res. **115**, D00H19 (2010), doi:10.1029/2009JD012147.
41. B. Chen, J. Huang, P. Minnis, Y. Hu, Y. Yi, Z. Liu, D. Zhang, and X. Wang, "Detection of dust aerosol by combining CALIPSO active lidar and passive IIR measurements," Atmos. Chem. Phys. **10**(9), 4241–4251 (2010).

1. Introduction

Dust play an important role in global climate by scattering and absorbing solar and terrestrial radiation, thereby influencing the radiation balance in the atmosphere [1–5]. The global largest dust source is the Saharan, from where considerable amounts of dust are frequently transported over Atlantic Ocean and the Mediterranean and Caribbean Seas towards South America and Europe [6]. Asian dust often originates from the Taklimakan and Gobi deserts in late winter and spring. This dust is transported long distances by the prevailing westerlies, passing over northeastern Asia and the Pacific Ocean, and reaching North America [7–10]. Asian dust was found to have made more than one full circuit around the globe within 13 days after being lifted to the upper troposphere [11]. Dust can also be transported to the Tibetan Plateau by topographic lifting [12, 13]. During transport, dust not only reduce local air quality, affect human health and carry the bacilli [14–17], but also act as ice nuclei (IN) and condensation nuclei (CCN) of clouds, thus changing the radiative properties of clouds, ice water paths, precipitation, and cloud lifetimes [3,18–21]. Furthermore, dust can act as nutrients for marine biological organisms and modulate the ocean–atmosphere carbon cycle when transported and deposited over the oceans [22, 23].

The Cloud-Aerosol Lidar and Infrared Pathfinder Satellite Observations (CALIPSO) satellite is a part of the A-Train constellation of satellites. The two-wavelength, polarization-sensitive backscatter LIDAR (CALIOP) onboard CALIPSO can provide global-scale, high-resolution vertical profiles of both clouds and aerosols within the Earth's atmosphere [24]. Comprehensive studies on the characterization of dust, such as the occurrence of dust plumes over the Tibetan region [12], dust generation, long-range transport [6, 10], height-resolved global or regional distribution [11, 25], and dust optical properties [26, 27], have been conducted based on CALIPSO measurements.

Hu et al. [28, 29] derived an empirical relationship between the multiple-scattering fraction and the linear depolarization ratio based on Monte Carlo simulations, and then accurately assessed the effect of multiple scattering on LIDAR data for water clouds. Furthermore, water cloud with positive slope and ice cloud with negative slope were identified from the layer-integrated attenuated backscatter coefficient and layer-integrated depolarization ratio relationship using CALIPSO LIDAR observations [30]. In addition, Cho et al. [31] studied the relationship between LIDAR layer-integrated attenuated backscatter coefficient and the corresponding layer-integrated depolarization ratio for nine International Satellite Cloud Climatology Project (ISCCP) cloud classes with different cloud top temperatures and latitude belts. They then compared the cloud phases determined using the layer-integrated attenuated backscatter coefficient - layer-integrated depolarization ratio relation from CALIPSO with results obtained from the Moderate Resolution Imaging Spectroradiometer (MODIS). In this study, we focus mainly on the difference between cloud and dust given by the relationship between the layer-integrated attenuated backscatter coefficient and layer-integrated depolarization ratio. On the basis of this relationship, we propose a simple improved algorithm for detection of dust plumes from CALIPSO observations. The rest of this paper is organized as follows. Sections 2 and 3 describe the data processing used in this study and compare the relationship between dust and cloud, respectively. Sections 4 and 5 present a case study and dust occurrence over East Asia derived from the proposed algorithm. Finally, we provide our conclusions in section 6.

2. Satellite data

2.1 CALIPSO lidar

The Cloud-Aerosol Lidar with Orthogonal Polarization (CALIOP) instrument was launched aboard the CALIPSO satellite in April 2006 and became operational in June 2006. CALIPSO is the first satellite carrying an elastic backscatter LIDAR with dual wavelengths (532 and 1064 nm) and polarization sensitivity (532 nm), to provide long-term continuous observation of cloud and aerosol on a global scale [24]. The vertical structure of clouds and aerosols retrieved by CALIOP offers an unexpected opportunity to study occurrence, properties, thin cirrus, cloud–climate feedbacks, spatial distribution and distance transport of dust [32]. CALIOP level 2 products describe physical properties of clouds and aerosols after atmospheric layers are first detected and identified as cloud or aerosol. The detail overview of more CALIPSO data products and CALIPSO mission was introduced by the Winker et al. [33]. In this study, the layer-integrated attenuated backscatter coefficient, layer-integrated depolarization ratio and Vertical Feature Mask products in the level 2 version 3 layer products were used to distinguish dust from cloud layers.

2.2 CloudSat

CloudSat, part of the A-Train constellation, was launched in 2004 providing much needed measurements of the vertical structure of cloud from space, similar to CALIPSO. The 94-GHz Cloud Profiling Radar (CPR) provides vertical profiles of the equivalent radar-reflectivity factor at approximately 1.5 km horizontal and 240 m vertical resolution [34]. Because the satellite uses microwaves with wavelengths on the order of a few millimeters, it has difficulty detecting aerosol particles, but its microwaves are scattered efficiently by cloud particles. To eliminate observations containing cloud, the CloudSat cloud mask from the 2B-GEOPROF products has been utilized.

2.3 Dust and cloud data processing

Table 1 summarizes the cases of dust, water cloud, and ice cloud selected in this study. Dust cases are limited to over dust sources (Taklimakan and Saharan deserts), and both water cloud and ice cloud are limited to over marine regions. The integrated attenuated backscatter coefficient and layer-integrated depolarization ratio for water and ice cloud were directly obtained from level 2, 1-km C-layer products, in which the maximum altitude is 20.2 km.

#188543 - $15.00 USD Received 9 Apr 2013; revised 27 May 2013; accepted 5 Jun 2013; published 18 Jun 2013

However, the same variables for dust were obtained from levels 1 and 2 data. The detailed processing of dust was as follows: First, the top and base of the dust layer were obtained from level 2, 5-km A-layer products. Second, the higher horizontal resolution of the dust-layer top and base height was output by converting from 5 km to 333 m. Third, the layer-integrated attenuated backscatter coefficient and layer-integrated depolarization ratio were calculated using Eq. (6.6) of Vaughan et al. [35] after atmospheric layers were detected in level 1 data, considering attenuation of the signal due to molecules and ozone at 532 and 1064 nm, respectively.

3. Comparison of the relationship between dust and cloud

Here, we attempt to find the layer-integrated attenuated backscatter coefficient and layer-integrated depolarization ratio relationship for dust and apply it to detect dust plumes. Figure. 1 depicts the relationship between the layer-integrated attenuated backscatter coefficient and the layer-integrated depolarization ratio for dust, water cloud, and ice cloud. Because the single scattering by water droplets does not depolarize backscattered light, multiple scattering events do tend to depolarize LIDAR signals within water cloud. Thus the layer-integrated depolarization ratio of water cloud shows quite large values and increases with layer-integrated attenuated backscatter coefficient. Polarization, however, is sensitive to non-spherical particles such as ice and dust. The lower right portion of the ice cloud (see Fig. 1, corresponding to layer-integrated depolarization ratio between 0.25 and 0.55) is associated with ice cloud that contains a large number of randomly oriented ice particles, and the upper left portion of the ice cloud showing high layer-integrated attenuated backscatter coefficient (between 0.08 and 0.14) and small layer-integrated depolarization ratio values was caused by horizontally oriented ice crystals which could lead the presence of specular reflection. The distribution of dust with low backscattered light and a wide range in depolarization ratio, recognized as non-spherical particles, is shown in the lower middle portion of Fig. 1. The obviously different distributions for dust, water cloud, and ice cloud can be readily seen. As we would expect, the distribution trends of water cloud and ice cloud agree closely with the results of Hu [30]; some differences may be caused by the differences in optical properties and the number of cases. What is surprising is the distribution of dust, the range of the layer-integrated attenuated backscatter coefficient and the layer-integrated depolarization ratio was supported by previous work [36, 37].

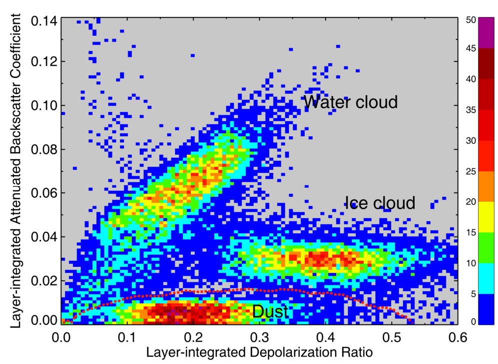

Fig. 1. The relationship between the layer-integrated depolarization ratio and the layer-integrated attenuated backscatter coefficient for dust, water clouds, and ice clouds. The color of each pixel represents the total number of points in a $\Delta\delta$-$\Delta\gamma$ box measuring 0.6×0.14 sr^{-1}. The red dotted line represents the layer-integrated Attenuated Backscatter Coefficient (ABC) threshold used to separate dust from cloud.

This distribution of dust exhibits a marked difference that could be used to distinguish dust from cloud. The threshold marked by the red dotted line in Fig. 1 was established from the layer-integrated attenuated backscatter coefficient and the layer-integrated depolarization

Received 9 Apr 2013; revised 27 May 2013; accepted 5 Jun 2013; published 18 Jun 2013

ratio. However, the layer-integrated attenuated backscatter and layer-integrated depolarization ratio alone may not be sufficient to distinguish dust from cloud. A histogram distribution of the layer-integrated color ratio for cloud and dust plumes, which is very similar to results of Vaughan [38], is shown in Fig. 2. The peak value was approximately 0.6 for dust and about 1.1 for cloud, including both water and ice cloud. Thus, the value of 0.76 of the layer-integrated color ratio could also be used as another threshold for distinguishing dust from cloud. Although the most of dust and cloud could be accurately identified using the layer-integrated color ratio threshold, the overlap value between 0.6 and 0.9 may cause ambiguity in attempting to distinguish the dust and cloud through a layer-integrated color ratio approach alone.

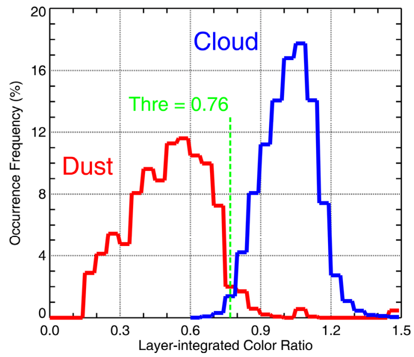

Fig. 2. Histogram of the integrated color ratio for dust (red line) and cloud (blue line), the green line indicates the threshold used to separate dust from cloud.

As described above, combining the layer-integrated depolarization ratio–layer integrated attenuated backscatter coefficient relationship and the threshold for the layer-integrated color ratio will greatly improve the ability to identify dust plumes. The procedure for detecting dust plumes is as follows: First, if the layer-integrated color ratio is little than 0.76, the feature layer is identified as a dust layer; otherwise, the feature layer is further identified. Second, the feature layer is considered a dust layer if the layer-integrated attenuated backscatter coefficient is smaller than the threshold for the same layer-integrated depolarization ratio. Note that the similarity in optical properties of thin cirrus and of dust was not considered in this study. As noted by Cho et al. [31], although the low attenuated backscatter coefficient and high depolarization ratio of optically thin ice cloud are similar to those of dust, the dust layer could be successfully identified by combined use of the threshold of the layer-integrated color ratio and the relationship of the LIDAR backscatter and depolarization ratio. As a result, the accuracy of the proposed method for detection of dust plumes would be not affected significantly by optically thin cirrus.

4. Example: identification of dust

An algorithm that can effectively and accurately distinguish dust from cloud is of significant importance for CALIPSO products. The currently used algorithm can identify dust and cloud well, based on three-dimensional probability distribution functions (PDFs) of attenuated backscatter, the layer-integrated color ratio, and the mid-layer altitude [39]. Researchers have proven that the algorithm is a reliable operational approach. However, as pointed out by Liu et al. [39], there are still a few cases of misclassification of dust and cloud. For example, a very dense dust layer near or over a source region could be misclassified as cloud by this approach. Misclassification of dust as cloud has been obtained and discussed over Saharan dust source region by Pappalardo et al. [40] based on the framework of EARLINET correlative measurements for CALIPSO. To address this problem, Chen et al. [41] proposed a method that could successfully reduce the percentage of misclassified dense dust layers from

43% to 6.7%. Their method involves combining measurements of the active LIDAR CALIOP and the passive Infrared Imaging Radiometer (IIR) launched aboard the CALISPO satellite. In the following, we show the advantage of our introduced approach and compare the results to coincident observations of CloudSat and the vertical feature mask of the CALIOP data algorithm.

The CPR and CALIOP complement each other well in providing global three-dimensional aerosol and cloud structure because of their advantage of each observing a different set of wavelengths. The cloud mask derived from the coincident CloudSat radar measurements, the total attenuated backscatter and depolarization ratio measured by CALIOP at 532 nm, and the CALIOP vertical feature mask (VFM) are presented in Figs. 3(a)–3(d), respectively. A very dense dust plume, observed by CALIOP over the Taklimakan Desert on 30 July 2006, was misclassified as water cloud in CALIPSO VFM products. On the other hand, the dust plumes were not observed by CloudSat because the dust particles were quite small compared with the radar wavelength (millimeter size).

In the present study, the VFM data between 35.2°N and 45°N were inferred. The heights of the cloud feature layer top and base were found from a profile of the VFM. Multiple layers were presented when the gap between cloud feature layers was greater than 16 bins at the vertical profile. Then, both thresholds were used after the integration of the cloud feature layer top and base. The modified VFM is shown in Fig. 3(e), and the dust plumes were identified correctly from 35.2°N to 45°N. Some vertical bars where the color index equals 2 in Fig. 3(e) were produced by the default value in the calculation for dust layer-integrated color ratio.

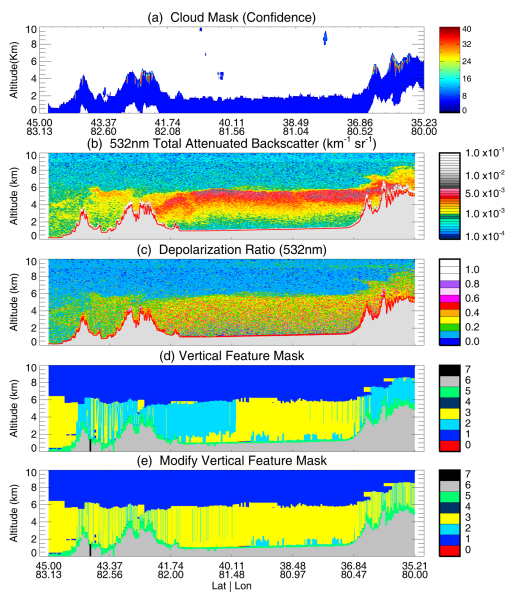

Fig. 3. Vertical distribution of clouds and aerosols observed by CALIPSO and CloudSat over the Taklimakan Desert on 30 July 2006: (a) CloudSat cloud mask image, (b) CALIPSO 532 nm total attenuated backscatter coefficient; (c) CALIPSO 532 nm volume depolarization ratio; (d) CALIPSO vertical feature mask; (e) new vertical feature mask from the proposed method in this study. The color bar of the VFM indicates the type of particle layer: 0 = invalid, 1 = clear air, 2 = cloud, 3 = dust, 4 = stratospheric layer, 5 = surface, 6 = subsurface, 7 = totally attenuated.

5. Distribution of dust

To better understand dust transport in three dimensions over East Asia, the vertical distribution of dust occurrence over the region 30°N–45°N, 80°E–180°E was derived by the

#188543 - \$15.00 USD Received 9 Apr 2013; revised 27 May 2013; accepted 5 Jun 2013; published 18 Jun 2013

proposed method using the night measurements from March to May, 2007. As shown in Figs. 4(a)-4(d), the dust occurrence is defined as the ratio of the number of dust layer features to the number of layer features (cloud and dust layer) and clear air in the i-th bin at vertical direction. The results of zonal and meridional mean occurrence for modify VFM and CALIPSO VFM showed that dust occurrence decreases significantly with altitude. Dust can be found up to around 6–8 km (ASL) near the Taklimakan Desert (36°N–40°N, 80°E–110°E) region. Furthermore, the zonal distribution of dust was divided into two main parts in Figs. 4(a)-4(b). One part with altitude above 1 km (ASL) over the region 33°N–42°N in the Figs. 4(a)-4(b), the highest altitude up to 8 km (ASL), was caused mainly by the Taklimakan dust and transport-path dust crossing over the surrounding mountains and being transported eastward under the influence of meteorological conditions. The other part with altitude below 1 km (ASL) over the region 30°N–41°N was attributed by the descending of dust far away from the dust source region. From the meridional distribution perspective (Figs. 4(c)-4(d)), most of the dust occurs below 4 km (ASL). Maximum dust occurrence is over 80% above the Taklimakan dust source region (80°E–110°E). During the transport period, the altitude of transported dust decreases significantly with increasing longitude until 140°E, and occurrence also gradually decreases. As can be clearly seen in the Fig. 4(d), the transport altitude remained at 3–7 km (ASL) as the dust was transported across the Pacific Ocean (30°N–45°N, 140°E–180°E). The spatial distribution of dust with longitude confirms the two parts discussed above.

As shown in Figs. 4(a)-4(d), the dust occurrence over East Asia has been compared between the proposed method and CALIPSO's method. It is clear seen that the dust occurrence obtained from the proposed method is larger than that of the CALIPSO's method in the Figs. 4(a)-4(d). The maximum occurrence below 1km (ASL) is up to 50%-60% and 40%-50% for proposed method and CALIPSO's method over the 30°N-42°N region, and that of above 1km (ASL) is up to 40%-50% and 30%-40% for both methods, respectively. In the longitude view, there are two main parts. On the one hand, it is seen that the difference of dust occurrence was shown over dust source region (80°E-100°E) at the range of 4km to 6km (ASL); on the other hand, the dust occurrence over the Pacific ocean region (140°E −180°E) was separated into two layers. The maximum occurrence for the bottom layer with altitude below 2km (ASL) is 20%-40% and 0%-10%, respectively. More vertical region distributed by the dust in the upper layer with the range of 3km to 8km (ASL) could be found. As shown in the results above, the two possible causes were explained by following. Firstly, the proposed method can identify well dust plumes misclassified as cloud over the dust source region; Secondly, when the more cases were analyzed by us in this work, few clouds were misclassified as dust. So, it can also contribute to the dust occurrence.

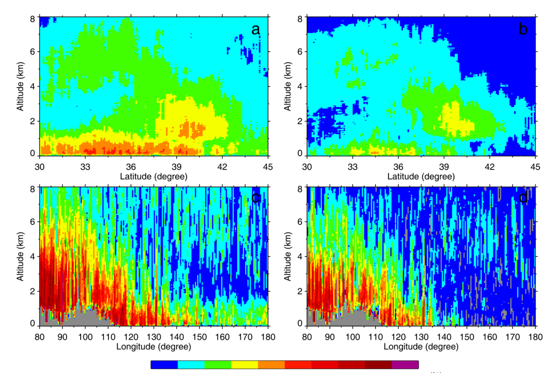

Fig. 4. Vertical distributions of the zonal (upper) and meridional (bottom) mean dust occurrence for modify VFM (left) and CALIPSO VFM (right) obtained by the proposed method and CALIPSO's method over the East Asian region (30°N–45°N, 80°E–180°E, Above Sea Level) from March to May, 2007.

Table 1. Summaries of selected cases of water cloud, ice cloud, and dust

Types	Cases	Date	Time (UTC)	Latitude (deg)	Longitude (deg)
Water cloud	1	04/11/2007	11:57	10.08- -22.29	-151.69- -148.93
	2	04/12/2007	07:53	-26.84- -8.60	-96.51- -92.33
	3	04/12/2007	09:20	15.79--21.89	-111.80- -110.40
	4	04/12/2007	10:59	15.80--21.90	-136.52- -135.12
	5	04/13/2007	11:46	3.13--21.44	-150.09- -146.04
	6	04/14/2007	10:46	8.83--21.05	-134.96- -132.23
	7	04/21/2007	07:43	-24.31- -12.12	-94.33- -91.54
	8	04/23/2007	07:29	-20.0- -6.80	-90.0- -87.29
	9	04/27/2007	07:07	-32.47- -14.26	-87.14- -82.73
	10	05/06/2007	21:02	18.50--24.56	-113.72- -112.30
	11	05/06/2007	22:41	12.47--24.63	-138.46- -137.03
	12	05/08/2007	22:56	19.12--25.17	-135.50- -134.07
Ice cloud	1	03/01/2007	01:19	-26.66- -14.48	-171.60- -168.74
	2	03/02/2007	21:44	-44.01- -31.94	-114.84- -111.16
	3	03/03/2007	11:47	20.63--38.87	-147.78- -142.96
	4	03/03/2007	00:03	-49.59- -43.64	-146.82- -144.56
	5	03/05/2007	00:56	-31.08- -6.71	-167.11- -161.42
	6	03/08/2007	22:45	-35.49- -23.35	-132.47- -129.31
	7	03/12/2007	00:00	-30.70- -15.49	-152.83- -149.35
	8	03/13/2007	12:21	28.55--34.62	-155.12- -153.49
	9	03/15/2007	12:09	27.67--33.75	-152.26- 150.65
	10	04/07/2007	23:01	-23.00- -15.00	-137.20- -135.00
	11	04/15/2007	23:48	-31.46- -23.00	-148.00- -145.87
	12	04/16/2007	21:23	5.46--17.64	-118.29- -115.62
Dust	1	03/06/2007	20:28	38.53--41.49	85.62--86.55
	2	03/15/2007	20:22	38.51--39.99	87.13--87.59
	3	04/14/2007	20:34	37.52--42.00	83.75--85.16
	4	05/07/2007	20:41	37.33--39.76	82.16--82.81
	5	05/16/2007	20:33	37.85--41.54	83.84--85.00
	6	06/10/2007	20:27	37.48--39.50	85.25--85.87
	7	05/13/2007	01:59	17.72--23.79	-1.65- -0.23
	8	05/22/2007	00:15	17.78--21.80	24.61--25.54
	9	05/24/2007	01:42	15.29--21.39	2.41--3.81

6. Conclusions

In this study, an important relationship was obtained between the layer-integrated attenuated backscatter coefficient and layer-integrated depolarization ratio for dust with a low layer-integrated attenuated backscatter coefficient and a wide range of the layer-integrated depolarization ratio, which is unlike the distribution of water cloud with a positive slope and ice cloud with a negative slope. The histogram distribution of the layer-integrated color ratio for dust and cloud was also presented. The large difference between dust and cloud could be used to study the discrimination of dust and cloud. Thus, a simple inversion for detection of dust from CALIPSO measurements was developed based on the relationship between the layer-integrated attenuated backscatter coefficient and layer-integrated depolarization ratio, and using the layer-integrated color ratio. A dust case misclassified by current CALIPSO products was used to validate the proposed method, with the results suggesting that the proposed method can complement the current CALIPSO discrimination algorithm, especially over dust source regions. The zonal and meridional mean occurrence from the proposed method and the CALIPSO's method were compared over East Asia region (30°N-45°N, 80°E-180°E). The comparison showed that the dust occurrence obtained from the proposed method is larger than that of CALIPSO's method. The dust could be found up to around 6-8 km (ASL) near the Taklimakan desert region, and maximum occurrence is over 80%. The transport altitude remained at 3-7km (ASL) as the dust was transported across the Pacific Ocean.

The application of methods for dust identification and characterization was necessary over different dust source regions, long-transported pathway even over the global. Although the misclassified dust was identified well by the proposed method in this work, it still needs to be improved against more limitations and weakness. As described in previous, only the dust in this work was considered. The proposed method should be applied in more general complex situations where dust, cloud, and other aerosol types are mixed. The more parameters and scenes of the discrimination of dust from other type aerosols will be also needed. Meanwhile, due to the change of CALIOP pointing angle, the special thresholds of layer-integrated attenuated backscatter coefficient, layer-integrated depolarization ratio and layer-integrated color ratio based on the different training data set were obtained in our future work. The difference between the distributions of cloud and dust is also expected to be useful for studying the different properties of pure cloud and dusty cloud, as well as dust that has been misclassified as a cloud layer.

Acknowledgments

This research is supported by National Basic Research Program of China (2012CB955301) and National Natural Science Foundation of China (41205014). CloudSat Data were obtained through the CloudSat Data Processing Center (http://www.cloudsat.cira.colostate.edu). CALIPSO data have been obtained from the Atmospheric Sciences Data Center (ASDC) at NASA Langley research center.